

Geometry and Electronic Coupling in Perylenediimide Stacks: Mapping Structure–Charge Transport Relationships

Josh Vura-Weis, Mark A. Ratner,* and Michael R. Wasielewski*

Department of Chemistry and Argonne-Northwestern Solar Energy Research (ANSER) Center, Northwestern University, Evanston, Illinois 60208-3113

Received September 12, 2009; E-mail: ratner@chem.northwestern.edu; m-wasielewski@northwestern.edu

Polycyclic aromatic molecules have shown great promise in organic thin film transistors (OTFTs) and organic photovoltaics (OPVs) due to their tendency to form well-ordered π stacks in the solid state that act as efficient conduits for electron or hole transport.¹ Most organic electronic devices are fabricated through either vapor deposition or solution-based methods such as spin-casting, which is often followed by annealing to improve crystallinity. Defects such as grain boundaries and amorphous regions decrease device performance, in some cases by orders of magnitude.² The molecule–electrode interface can also affect efficiency. These variables make it difficult to determine whether the performance of a given device is inherent to the molecule itself or is due to problems with fabrication. Therefore, molecules with high intrinsic mobilities may be overlooked due to initial processing difficulties.

In this communication we use Density Functional Theory (DFT) to map the relation between stacking geometry, binding energy, and electronic coupling for the common organic semiconductor perylenediimide (PDI) and then use this method to screen 20 PDI derivatives and predict which will show the highest charge mobilities in ideal devices. PDI is a promising organic semiconductor due to its low price, robustness, high solar absorbance for OPV applications, and ability to form well-ordered π -stacked aggregates. Due to nodes in both the HOMO and LUMO along the long axis (Figure 1b), substitution at the imide position (R in Figure 1a) has a negligible effect on the optical and electronic properties of an isolated PDI molecule. However, this substitution changes its intermolecular interactions, leading to a wide range of nanoscale structures including liquid crystals³ and 1-D nanocrystals.⁴ PDI OTFTs have been created with electron mobilities as high as 1.4 cm²/(V s).⁵

While traditional DFT functionals such as B3LYP perform poorly for noncovalent interactions such as π – π stacking, the M06 family of functionals⁶ has been shown to give accurate geometries and energies for a variety of dispersion-dominated systems such as DNA base pair stacks⁷ and benzene aggregates. The dispersion-corrected DFT-D method is similarly effective and has recently been used to map the ground and excited-state potential surfaces of a PDI π -stacked dimer.⁸ These methods are much more computationally efficient than those traditionally used to study π – π stacks such as MP2 and CCSD. We have calculated the BSSE-corrected⁹ binding energy of a PDI dimer with R=H as a function of short-axis (x) and long-axis (y) displacement using the M06-2X functional with the 6-31++G** basis set in Q-Chem 3.1¹⁰ (ζ fixed at 3.5 Å). At each geometry the electronic coupling matrix elements for hole transport V_H and electron transport V_L were determined using the symmetric dimer energy-splitting method¹¹ (Figure 1c). In the Marcus regime, these couplings determine the efficiency of charge transport along a chain of molecules, with the rate of each hopping

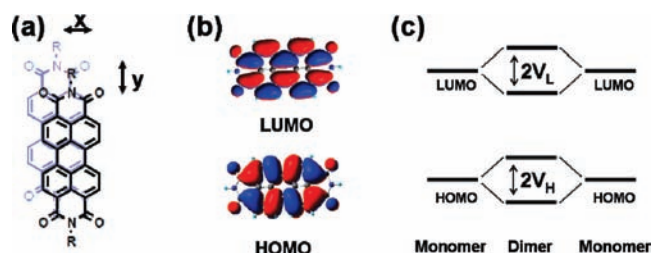


Figure 1. (a) Diagram of PDI stack displaced 1.5 Å along the short (x) axis and 2.5 Å along the long (y) axis. (b) HOMO and LUMO of PDI-H monomer. (c) Energy-splitting model used to calculate V_H and V_L .

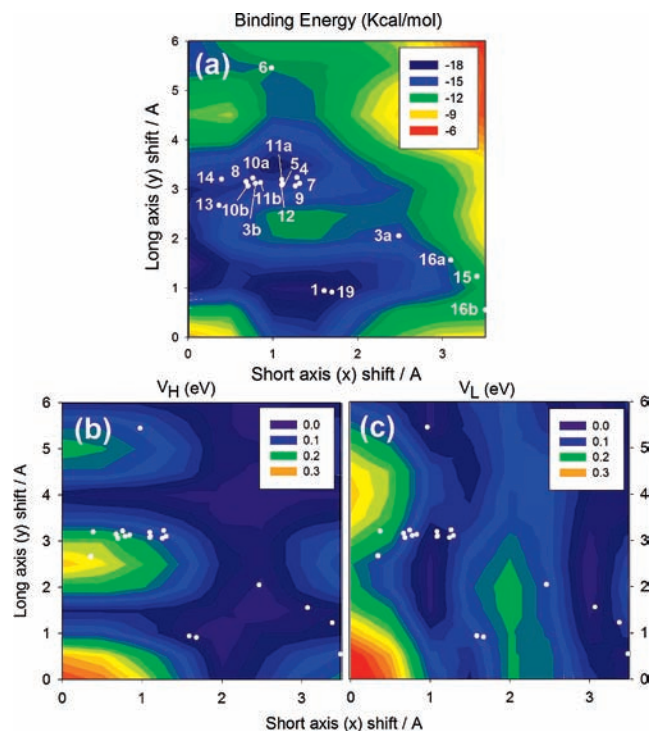

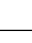
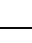
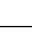
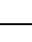

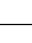

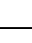
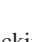


Figure 2. Binding energy (a) and electronic coupling for hole (b) and electron (c) transfer of PDI dimers vs stacking geometry ($\zeta = 3.5$ Å). White dots and labels indicate crystal geometries of molecules in Table 1.

step proportional to V^2 . In this work we neglect the reorganization energy, which is not straightforward to calculate in extended crystals.¹²

The binding energy and electronic coupling are shown in Figure 2 as a function of (x,y) displacement. The energy is dominated by nuclear repulsion, with the local maximum at approx (1.5, 2.5) corresponding to superposition of the imide region of one monomer with the top of the perylene region of the other (Figure 1a). Two broad minima at $y \approx 1-2$ and $y \approx 3-4$ indicate a large range of

Table 1. Electronic Coupling Matrix Elements for PDI Derivatives

#	R	V_H (eV)	V_L (eV)
1	—CH ₃	0.04	0.14
2	—CH ₂ Cl ₃	0.09, 0.09	0.01, 0.03
3	—(CH ₂) ₂ CH ₃	0.04, 0.20	0.20, 0.10
4	—(CH ₂) ₄ CH ₃	0.15	0.07
5	—(CH ₂) ₇ CH ₃	0.17	0.07
6	—CH ₂ CH(CH ₃)CH ₂ CH ₃	0.14	0.03
7	—CH ₂ CH ₂ OCH ₂ CH ₃	0.13	0.05
8	—(CH ₂) ₃ OCH ₃	0.19	0.13
9	—(CH ₂) ₃ OCH ₂ CH ₃	0.15	0.05
10	—(CH ₂) ₃ CH ₂ OH	0.19, 0.19	0.13, 0.11
11	—(CH ₂) ₄ CH ₂ OH	0.15, 0.19	0.01, 0.08
12	—CH ₂ — 	0.16	0.00
13	—CH ₂ —  —OCH ₃	See note ¹⁶	0.16
14	—CH ₂ CH ₂ — 	0.12	0.14
15	—CH ₂ CH(CH ₃)— 	0.01	0.07
16	—  —OCH ₂ CH ₃	0.03, 0.12	0.01, 0.04
17	—  —N=N— 	0.08	0.10
18	—  N	0.03	0.09
19	—  N	0.04	0.16
20	—  N	0.08	0.04

energetically accessible stacking geometries. Substitution at the imide positions will provide additional intermolecular interactions that can shift the preferred geometry along these valleys.

The electronic coupling for hole (electron) transport is governed by the overlap of monomer HOMO (LUMO) orbitals. While calculation of electronic coupling as a function of one geometric variable (x shift, y shift, or rotation) is common,¹³ the two-dimensional approach used here can identify regions of high coupling that might otherwise be missed, such as the peak in V_L at (2,2). Further insight is gained from side-by-side inspection of the binding energy and electronic coupling maps. The shallow valleys in the binding curve span geometries with very different couplings. For example, V_H ranges from 0.02 to 0.22 eV along $y = 3.0$ and V_L ranges from 0.02 to 0.29 eV along $y = 1.0$, in both cases with binding energy differences <3.5 kcal/mol. As the charge transfer rate is proportional to V^2 , we can therefore expect up to 100x changes in mobility through PDI crystals with various imide substituents simply due to different stacking geometries, though this range could be lessened by thermal fluctuations.¹²

We have calculated values of V_H and V_L for the 20 PDI derivatives¹⁴ listed in Table 1 using the (x,y,z) shifts from the crystal structures and labeled the (x,y) shift of each in Figure 2.¹⁵ Five derivatives form crystals with pairs of inequivalent stacks (see Figure S1). Coupling values for both stacking geometries are listed in the table and are labeled in Figure 2 (e.g., **3a**, **3b**). All but three crystal structures adopt geometries in the broad minima of the binding surface, indicating that except in the case of bulky substituents such as **6**, **15**, or **16** the stacking is dominated by interactions between PDI cores.

PDI OTFTs can exhibit ambipolar behavior,¹⁷ and Table 1 identifies several derivatives with high coupling for both e^- and h^+ transport. Molecules **19**, **13**, **14**, and **1** have the highest V_L , and **8**, **10**, and **11** have the highest V_H . One of the inequivalent stacks of **3** has high V_H , while the other has high V_L ; this might suggest unusual transport mechanisms. Several derivatives have higher

coupling than the common organic semiconductor pentacene ($V_H = 0.10$).¹⁸ To our knowledge, only molecules **14**, **4**, and **5** have been incorporated into an OTFT device, with electron mobilities 1.4, 0.6, and 0.1 $\text{cm}^2/(\text{V s})$, respectively.⁵

In conclusion, we have used the recently developed M06-2X DFT functional to simultaneously map the binding energy and electronic coupling surfaces of PDI dimers and have shown that geometries with a large coupling for either e^- or h^+ transport are energetically accessible. We then calculated the coupling for 20 PDI derivatives and identified the most promising candidates for incorporation into devices such as OTFTs and OPVs. This strategy of side-by-side inspection of binding energy and coupling surfaces should prove valuable for other organic semiconductors such as pentacene¹⁹ and poly(thiophene) derivatives.

Acknowledgment. J.V.W. thanks Dr. Chad Risko for helpful discussions and the NSF GRFP. This work was supported by the Office of Naval Research Grant No. N00014-05-1-0021.

Supporting Information Available: Computational details, (x, y, z) shifts of molecules studied, full citation for ref 10. This material is available free of charge via the Internet at <http://pubs.acs.org>.

References

- (1) *Organic Field-Effect Transistors*; Bao, Z., Locklin, J., Eds.; CRC Press: Boca Raton, FL, 2007.
- (2) Huttner, S.; Sommer, M.; Thelakkt, M. *Appl. Phys. Lett.* **2008**, *92*, 093302.
- (3) Struijk, C. W.; Sieval, A. B.; Dakhorst, J. E. J.; van Dijk, M.; Kimkes, P.; Koehorst, R. B. M.; Donker, H.; Schaafsma, T. J.; Picken, S. J.; van de Craats, A. M.; Warman, J. M.; Zuilhof, H.; Sudholter, E. J. R. *J. Am. Chem. Soc.* **2000**, *122*, 11057–11066.
- (4) Zang, L.; Che, Y.; Moore, J. S. *Acc. Chem. Res.* **2008**, *41*, 1596–1608.
- (5) (a) Chesterfield, R. J.; McKee, J. C.; Newman, C. R.; Ewbank, P. C.; da Silva, D. A.; Bredas, J. L.; Miller, L. L.; Mann, K. R.; Frisbie, C. D. *J. Phys. Chem. B* **2004**, *108*, 19281–19292. (b) Oh, J. H.; Lee, H. W.; Mannsfeld, S.; Stoltenberg, R. M.; Jung, E.; Jin, Y. W.; Kim, J. M.; Yoo, J. B.; Bao, Z. N. *Proc. Natl. Acad. Sci. U.S.A.* **2009**, *106*, 6065–6070. (c) Briseno, A. L.; Mannsfeld, S. C. B.; Reese, C.; Hancock, J. M.; Xiong, Y.; Jenekhe, S.; Bao, Z.; Xia, Y. *Nano Lett.* **2007**, *7*, 2847. Crystal structures of some PDI OTFTs are not known.
- (6) Zhao, Y.; Truhlar, D. G. *Theor. Chem. Acc.* **2008**, *120*, 215–241.
- (7) Hohenstein, E. G.; Chill, S. T.; Sherrill, C. D. *J. Chem. Theory Comput.* **2008**, *4*, 1996–2000.
- (8) (a) Fink, R. F.; Seibt, J.; Engel, V.; Renz, M.; Kaupp, M.; Lochbrunner, S.; Zhao, H.-M.; Pfister, J.; Würthner, F.; Engels, B. *J. Am. Chem. Soc.* **2008**, *130*, 12858–12859. (b) Zhao, H.-M.; Pfister, J.; Settels, V.; Renz, M.; Kaupp, M.; Dehm, V. C.; Würthner, F.; Fink, R. F.; Engels, B. *J. Am. Chem. Soc.* **2009**, *131*, 15660–15668.
- (9) Boys, S. F.; Bernardi, F. *Mol. Phys.* **1970**, *19*, 553–566.
- (10) Shao, Y.; et al. *Phys. Chem. Chem. Phys.* **2006**, *8*, 3172–3191.
- (11) Bredas, J. L.; Beljonne, D.; Coropceanu, V.; Cornil, J. *Chem. Rev.* **2004**, *104*, 4971–5003.
- (12) Coropceanu, V.; Sánchez-Carrera, R. S.; Paramonov, P.; Day, G. M.; Brédas, J.-L. *J. Phys. Chem. C* **2009**, *113*, 4679–4686.
- (13) (a) Kazmaier, P. M.; Hoffman, R. *J. Am. Chem. Soc.* **1994**, *116*, 9684–9691. (b) Feng, X. L.; Marcon, V.; Pisula, W.; Hansen, M. R.; Kirkpatrick, J.; Grozema, F.; Andrienko, D.; Kremer, K.; Mullen, K. *Nat. Mater.* **2009**, *8*, 421–426. (c) Hutchison, G. R.; Ratner, M. A.; Marks, T. J. *J. Am. Chem. Soc.* **2005**, *127*, 16866–16881. (d) da Silva, D. A.; Kim, E. G.; Bredas, J. L. *Adv. Mater.* **2005**, *17*, 1072–1076.
- (14) (a) Klebe, G.; Graser, F.; Hadicke, E.; Berndt, J. *Acta Crystallogr., Sect. B* **1989**, *45*, 69–77. (b) Hino, K.; Sato, K.; Takahashi, H.; Suzuki, S.; Mizuguchi, J. *Acta Crystallogr.* **2005**, *e61*, o440–o441. (c) Mizuguchi, J.; Hino, K.; Sato, K.; Suzuki, S. *Acta Crystallogr.* **2005**, *e61*, o434–o436. (d) Mizuguchi, J.; Hino, K.; Sato, K.; Takahashi, H. *Acta Crystallogr.* **2005**, *e61*, o437–o439.
- (15) Monomers in **2**, **18**, and **20** are both translated and rotated in the stack, and are not shown on Figure 2.
- (16) The HOMO of this monomer contains a significant contribution from the methoxyphenyl orbitals, making the dimer-splitting model inappropriate. We thank Prof. Jean-Luc Bredas for alerting us to this.
- (17) Singh, T. B.; Erten, S.; Günes, S.; Zafer, C.; Turkmen, G.; Kuban, B.; Teoman, Y.; Sariciftci, N. S.; Icli, S. *Org. Electron.* **2006**, *7*, 480–489.
- (18) Cheng, Y. C.; Silbey, R. J.; da Silva, D. A.; Calbert, J. P.; Cornil, J.; Bredas, J. L. *J. Chem. Phys.* **2003**, *118*, 3764–3774.
- (19) Note that pentacene forms a herringbone structure, which requires a more complicated model; see discussion in the Supporting Information.

JA907761E